Ultrasonic process for the manufacture of proton exchange membrane fuel cell electrode assembly

Claire Tougne, Thomas Cavoué, Arnaud Morin, Christine Nayoze-Coynel

Journal of Power Sources 656 (2025) 238061

Contents lists available at ScienceDirect

Journal of Power Sources

journal homepage: www.elsevier.com/locate/jpowsour

Ultrasonic process for the manufacture of proton exchange membrane fuel cell electrode assembly

Claire Tougne, Thomas Cavoué, Arnaud Morin, Christine Nayoze-Coynel *

Univ. Grenoble Alpes, CEA, LITEN, 38000, Grenoble, France

HIGHLIGHTS

- Ultrasonic process reduces MEA assembly time by 94 %.
- Successful electrode transfers with 4 cm^2 and 24.6 cm^2 sonotrodes.
- Multilayer structures (up to 7 layers) assemblies validated with a 4 cm^2 sonotrode.
- Electrochemical tests show ultrasonic CCMs match conventional ones.

GRAPHICAL ABSTRACT

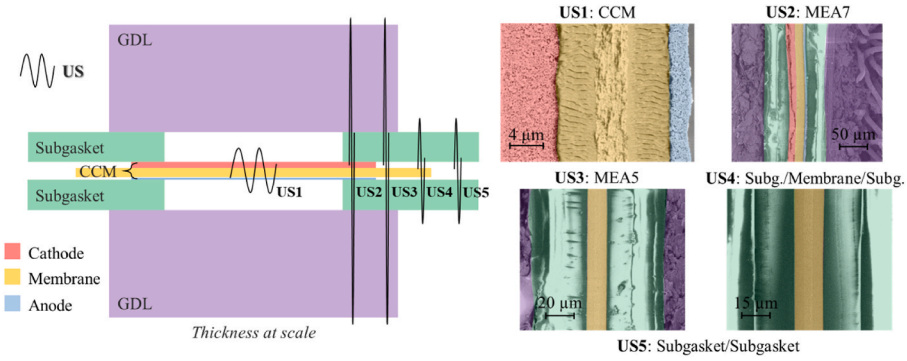

ARTICLE INFO

Keywords:
PEMFC
MEA
CCM
Ultrasound process
Decal transfer
Welding
Assembly

ABSTRACT

The growing demand for clean energy underscores the importance of Proton Exchange Membrane Fuel Cells (PEMFCs) as a sustainable electricity generation solution. However, their widespread adoption faces challenges in performance, durability, cost, and manufacturing efficiency. This study investigates the ultrasonic process as a rapid alternative to traditional methods for manufacturing Membrane Electrode Assemblies (MEAs). Unlike the slow and complex hot pressing method, the ultrasonic process assembles MEAs in seconds without external heating. It transfers pre-coated layers to form the Catalyst Coated Membrane (CCM) and welds components like gas diffusion layers (GDL) without additional adhesives.

This technique reduces assembly time by over 94 %, significantly enhancing production efficiency. Scanning Electron Microscope (SEM) analysis reveals that higher stress and energy input during the ultrasonic process decrease PTFE reinforcement thickness in the membrane (from 4.4 to 3.7 µm). Additionally, thanks to the SEM and X-ray tomography analyses, the weld quality is optimized by enabling detection and elimination of defects (distorted membrane, cracks and hole), ensuring defect-free interfaces.

Initial fuel cell tests in 1.8 cm^2 differential cell and 20 cm^2 technical mono-cell, confirm that MEAs produced via the ultrasonic process perform similarly to those made with conventional techniques, under dry (<50 % RH) and wet (>80 % RH) conditions at 80 °C. In the 20 cm^2 cell at 0.8 V, both MEAs deliver identical current

* Corresponding author.
E-mail address: christine.nayoze@cea.fr (C. Nayoze-Coynel).

https://doi.org/10.1016/j.jpowsour.2025.238061
Received 25 June 2025; Received in revised form 25 July 2025; Accepted 4 August 2025
Available online 15 August 2025

densities: 0.504 A/cm^2 (dry) and 0.305 A/cm^2 (wet). These results position ultrasonic process as a breakthrough in PEMFC manufacturing, offering a faster, more efficient process that supports the transition to clean energy.

1. Introduction

The growing global demand for energy and the urgent political need to reduce greenhouse gas (GHG) emissions highlight the importance of transitioning from fossil fuels to renewable or nuclear energy sources [1]. Proton Exchange Membrane Fuel Cells (PEMFC) are a promising technology for both transportation and stationary applications, producing only water and heat as by-products [2,3]. However, their widespread adoption is hindered by high costs, performance issues, and durability challenges [3].

Advancements in PEMFCs, including improved catalysts, membrane materials, and system designs, have enhanced performance and longevity while reducing costs. Innovations in assembly techniques, such as advanced catalyst layers and flow field designs, have further cut production costs and boosted efficiency [4–7].

The traditional method for manufacturing Membrane Electrode Assemblies (MEAs) involves producing the Catalyst-Coated Membrane (CCM) and assembling it with Gas Diffusion Layers (GDLs) and subgasket components. The CCM can be prepared by direct catalyst deposition techniques, including sputtering, silkscreen printing, or inkjet printing, or by the decal transfer method, which involves pre-coating the catalyst layers onto a temporary inert substrate that is then transferred onto the membrane [7,8]. This is followed by hot pressing (HP) to bond the CCM with GDLs and subgaskets [9,10]. During this process, GDLs are carefully aligned with the CCM and subgaskets to ensure mechanical stability and prevent leakage. Hot pressing requires specific molds, temperatures (100–170 °C), and pressing times (3–15 min) to ensure strong adhesion [7,10–12]. In some cases, additional adhesives may be used to enhance the bond between the GDLs and the subgaskets. The choice of adhesive and its application are crucial to ensuring durability and preventing potential degradation of the MEA's performance.

Recent developments have introduced ultrasonic (US) welding as an innovative assembly method [13–23]. This technique uses a sonotrode operating at ultrasonic frequencies (20–70 kHz) to generate localized frictional heat, welding components together quickly and efficiently. Ultrasonic welding offers precise control, is suitable for a wide range of thermoplastic materials [24–26], and many parameters can be controlled (ultrasonic amplitude, energy, welding force, time, etc.). No additional molds, embossing tools, positioning templates, or specific tooling is necessary, with the exception of the sonotrode and the anvil specifically designed for the ultrasonic machine and for the design to be welded.

The ultrasonic process is faster (seconds vs. minutes) and requires minimal equipment compared to hot pressing. For example, Beck and al. used 7.5–9 s to weld gas diffusion electrodes (GDE) to the membrane [13–15]. It eliminates the need for adhesives and external heating, making it ideal for large-scale production. Moreover, the ultrasonic process generates no material waste and the only heat generated is the one produced inside the material during their friction. This localized and low-energy input further enhances its efficiency and sustainability.

Several patents have been published in this field, including the decal transfer of electrodes to the membrane [16,21], GDE bonding with a membrane [17], welding of subgaskets onto the membrane [18,19], and welding of GDLs onto the other components [27]. The simultaneous bonding of multiple layers (from 2 to 7) of different natures within the MEA is possible without the use of release films. Furthermore, this type of process can be integrated into a production line, and the high production rate allows for efficient manufacturing [20].

The ultrasonic process appears suitable for assembling PEMFC MEA components, but optimizing parameters is crucial to produce MEAs with the required characteristics for proper cell operation. This paper presents the limits and optimized parameters for electrode transfer onto the membrane and welding of various MEA components using ultrasonic technology, along with preliminary results comparing an ultrasonic-manufactured CCM to one made by hot pressing.

2. Experimental

2.1. Ultrasound machine

Thanks to a Herrmann Ultraschall 35 kHz-1200 W machine (Fig. 1a), electrical energy is converted into mechanical vibrations using a vibratory unit. This unit consists of a transducer, a booster, and a sonotrode, as illustrated in Fig. 1b. The booster adjusts the ultrasound

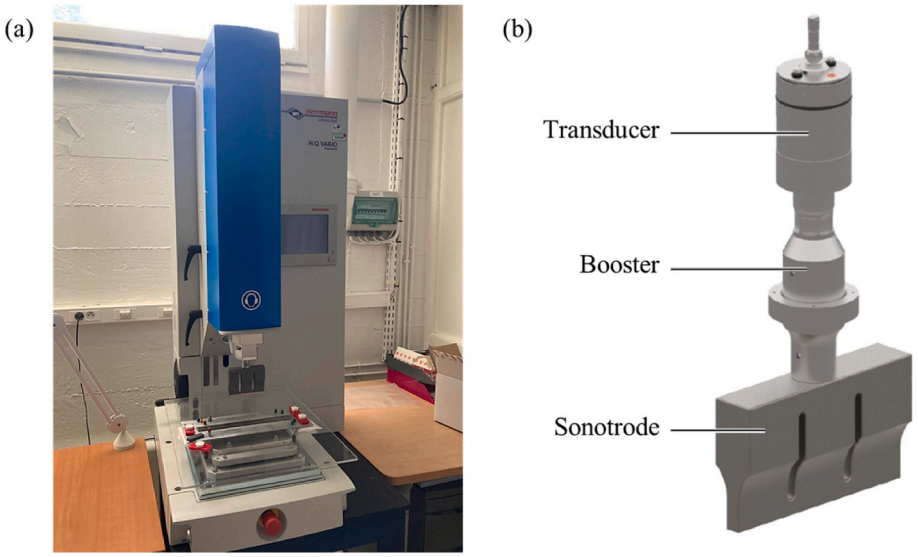

Fig. 1. (a) Picture of Herrmann Ultraschall 35 kHz-1200 W machine, named HiQ G1 VARIO 35/1200, (b) Structure of the vibratory unit composed with a transducer, a booster and the 4 cm^2 sonotrode from the user manual of Herrmann Ultraschall.

amplitude, while the sonotrode transmits the vibration to the materials. Two rectangular sonotrodes with different sizes have been used in the study: a 4 cm^2 (0.4 × 10 cm) and a 24.6 cm^2 (7.7 × 3.2 cm). Photos of each sonotrode, along with their corresponding anvils, are provided in Supplementary Fig. S1. The 4 cm^2 sonotrode was employed to demonstrate the proof of the concept for different welds, while the 24.6 cm^2 sonotrode was used to evaluate the performance of CCMs manufactured by ultrasound process (CCM-US) in a single-cell test. The use of the ultrasonic machine requires hearing protection due to noise levels. The average sonotrode lifetime is around 10–15 million cycles, based on packaging industry data. However, durability with our specific materials and conditions remains to be fully evaluated.

Concerning the ultrasound-assembled MEA, designed for a 20 cm^2 cell, it was manufactured using a more powerful Herrmann Ultraschall machine (20 kHz-6200 W). The sonotrode used has a frame shape with external dimensions of 4.1 × 11.3 cm and internal dimensions of 3.3 × 7.8 cm, and therefore a surface area of 20.6 cm^2. This sonotrode consists in welding the boarder of the GDL onto the subgasket.

The main parameters of the ultrasonic process include ultrasonic amplitude (μm), energy (J), welding force (F1 or F1-F2; N), control of the transition from F1 to F2, time (weld or stop; s), trigger force (N), start force (N), activation of the oscillator up or down and power (W). They will vary depending on the types of welds.

2.2. MEA manufacturing

2.2.1. Electrode preparation

CCMs consist of electrodes (anode and cathode) manufactured from a single ink formulation. The ink is composed of a platinum/carbon catalyst (TEC10E50E Tanaka®), a Nafion® ionomer (D2020) with an ionomer/carbon ratio of 1.1, and a water/ethanol mixture at a ratio of 3. In a flask, the platinum/carbon catalyst is mixed with water and ethanol, followed by the ionomer dispersion. Zirconia beads with a diameter of 3 mm are added to the ink to facilitate thorough mixing. The flask is then placed on roller mixer during 12 h. Finally, the catalytic ink is applied to an inert Teflon support, heated at 60 °C on a coating table (Elcometer). The catalyst loading is checked through X-ray fluorescence spectrometry (XVD-SDD from Fisher Technology). The anode is loaded at 0.1 ± 0.02 $mgPt/cm^2$ and the cathode at 0.3 ± 0.02 $mgPt/cm^2$.

2.2.2. Catalyst Coated Membrane (CCM)

To manufacture a CCM-US, the electrodes on their inert support are positioned on either side of a membrane (Gore® M820.15) and transferred via ultrasonic process or hot press, a conventional process. The two rectangular sonotrodes have been used for the decal transfer. The ranges of parameters applied depend on the sonotrode used. For the 4 cm^2 sonotrode, the tested ultrasound amplitude ranged from 17.9 to 22.4 μm, energy from 25 to 125 J/cm^2, and stress from 0.075 to 1.25 MPa. For the 24.6 cm^2 sonotrode, the tested ultrasound amplitude ranged from 11.7 to 19.5 μm, energy from 4 to 290 J/cm^2, and stress from 0.08 to 0.2 MPa.

Due to its shape of 0.4 cm × 10 cm, the CCM-US made with the 4 cm^2 sonotrode does not permit fuel cell tests because a surface of 1.2 × 1.5 cm^2 is required (1.8 cm^2 active surface). In consequence, only CCM-US manufactured with the 24.6 cm^2 have been tested in a 1.8 cm^2 differential cell. The performances of these CCMs will be compared to a CCM made by hot pressing (CCM-HP) using same membrane and electrodes. The CCM-HP was produced using a 3R SYNTAX press at 145 °C with a stress of 1 MPa for 180 s.

2.2.3. Membrane-electrodes assembly (MEA)

MEAs are composed of a variety of materials, including GDL, (Freudenberg H14CX653 comprising a carbon microporous layer (MPL) and carbon fibres with a polytetrafluoroethylene (PTFE) binder), polyethylene naphthalate (PEN) subgaskets (25 μm PEN + 22 μm of thermoactivable glue), perfluorosulfonated acid (PFSA) based membrane (Gore® M820.15), and the previously described CCM. Four types of welds are present in a MEA: GDL/subgasket/CCM/subgasket/GDL (US2, also named MEA 7), GDL/subgasket/membrane/subgasket/GDL (US3, also named MEA 5), subgasket/membrane/subgasket (US4) and subgasket/subgasket (US5). All these welds were realized using ultrasound with the 4 cm^2 sonotrode. The tested parameters for ultrasound amplitude ranged from 17.9 to 22.4 μm, energy from 25 to 200 J/cm^2, and stress from 0.25 to 2.0 MPa.

Two MEA were designed for a 20 cm^2 cell. The MEA-US is from a 24.6 cm^2 CCM-US (US1 zone) and the assembly of the GDL onto the subgasket (welding where all the components are superimposed like in US2) using 100 J/cm^2 with a stress of about 0.5 MPa parameters. The MEA-HP is from a CCM-HP and the assembly of the GDL and the subgasket also made by hot press. All the components are first pre-cut to the specific shapes of the 20 cm^2 cell (gas and cooling holes).

2.3. Quality of the assemblies produced

2.3.1. Optical microscopy

To establish the initial criteria for effective electrode transfer onto a membrane, observations were conducted using an Olympus DSX10 miscroscope. The microscope was used to measure the area of the electrode that was absent from the inert support following the ultrasound decal transfer process. The images obtained were processed in grayscale and then analyzed by thresholding to quantify the number of white pixels corresponding to the transferred surface. Ratios were calculated based on the sonotrode used, as per Equation 1.

$$Transferred\ surface\ (\%) = \frac{Missing\ surface\ on\ the\ inert\ surpport}{Surface\ of\ the\ sonotrode} \times 100$$

2.3.2. Scanning electron microscopy (SEM)

The SEM observations were carried out using a ZEISS NVISION40X1 to evaluate the quality of the transfer in CCMs or the welds in MEAs. The objective was to observe the interface between the components and to evaluate the thickness of the membrane in CCMs. Samples were trimmed and cut with a LEICA EM UC7 cryo-ultramicrotome at −120 °C to produce a flat surface for the SEM observations. CCMs and MEAs were cut without epoxy embedding and secured in a vice, avoiding any possible chemical contamination. The CCM thickness is about 29 μm (4 μm anode + 15 μm membrane + 10 μm cathode).

To prevent damage to the knife, it is necessary to remove the GDL component. In some cases, MPL of the GDL remained stuck to the membrane or electrode when the GDL was removed, resulting in a MEA thickness of approximately 175–200 μm (15 μm membrane or 30 μm CCM + 47 × 2 μm subgaskets + few tens of μm MPL). This precludes effective analysis of the membrane or electrode/MPL interface using a SEM. Consequently, a combined approach utilizing SEM in conjunction with X-ray tomography was employed.

2.3.3. X-ray tomography

X-ray tomography was used alongside SEM to image the interface between the membrane or electrode and MPL of GDLs in MEAs. Samples were cut into a triangular shape, glued onto a graphite stick, and fixed in a spinning sample holder to provide a volumetric view of the weld.

X-ray computed tomography of MEA 5 was performed at the ANATOMIX beamline of the Soleil synchrotron [28,29]. The setup included a 10 keV X-ray energy, a lutetium aluminum garnet scintillator, a 20x Mitutoyo objective, and a Hamamatsu Orca Flash 4.0 V2 sCMOS detector, with an effective voxel size of 323 nm. A total of 2000 projections were acquired over 180° with a 300 ms acquisition time. Tomographic reconstruction was done using PyHST2 software [30].

X-ray nano-tomography of the MEA 7 samples was conducted at the ID16B beamline [31] of the European Synchrotron Radiation Facility (ESRF) using a 29.6 keV pink beam. Four tomographic scans were performed at different propagation distances (holo-tomography technique

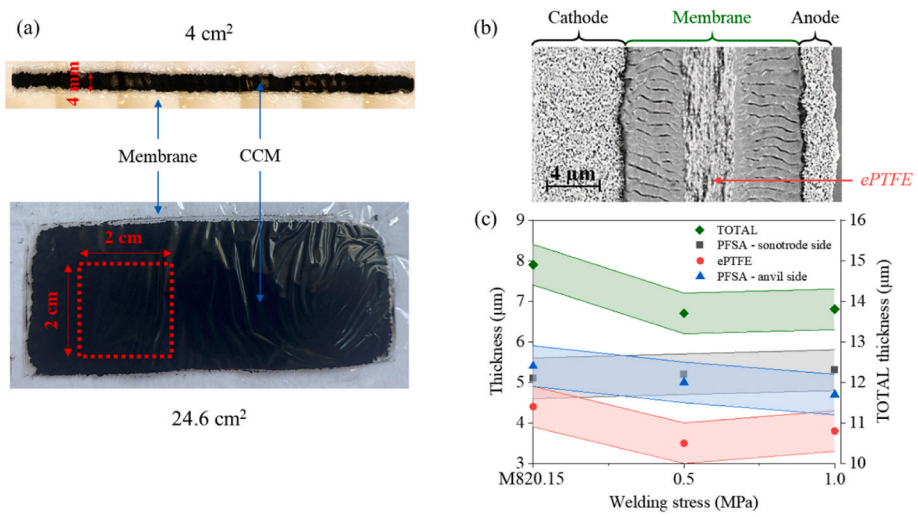

Fig. 2. (a) Ultrasound-assembled CCMs of varying sizes (4 and 24.6 cm^2), (b) Cross-Section of an ultrasound-assembled CCM by SEM, and (c) Membrane thickness evolution (PFSA-ionomer and ePTFE) as a function of applied stress up to 1 MPa at 75 J/$cm.^2$.

[32]), each acquiring 2505 projections over 360° with a PCO edge 4.2 camera (2048 x 2048 pixels, 25 nm effective voxel size, 20 ms acquisition time per projection). Phase retrieval and reconstruction were performed using PyNX [33] and Nabu [34].

2.3.4. Electrochemical performances

A preliminary comparative study was conducted between CCM-US and CCM-HP to ensure that the ultrasonic process for electrode transfer onto the membrane does not significantly affect CCM performance. No reproducibility tests were conducted on the results presented here; however, a more detailed study will be conducted in a subsequent paper.

CCMs were placed between two PEN subgaskets and two GDLs in a single fuel cell with an active area of 1.8 cm^2, named the differential cell. This cell consists of two identical graphite plates on the anode and cathode sides, with gas flow in a co-flow configuration. To ensure gas homogeneity at the inlet and outlet, fixed flow rates of 38 and 95 Nl/h were used, corresponding to a very large reactant stoichiometry of 50 at 1 A/cm^2 for the anode and cathode, respectively.

Performance was evaluated using polarization curves measured at 80 °C under two conditions: 90 % RH with 2.5 bar absolute (wet condition) and 40 % RH with 1.2 bar absolute (dry condition), under H_2 and air. The voltage was varied between OCV and 0.3 V with a scan rate of 2 mV/s.

High-frequency resistance (Rhf) was also measured using Electrochemical Impedance Spectroscopy in potentiostatic mode (PEIS). The cell was at open circuit voltage (OCV), with frequency oscillating from 100 Hz to 200 kHz and a 5 mV sinusoidal amplitude at 35 °C. Relative humidity varied from 20 % to 100 % in 20 % increments, using the same flow rates as previously mentioned, with hydrogen on the anode side and nitrogen on the cathode side at atmospheric pressure.

Preliminary tests in a 20 cm^2 technical single cell were carried out at 80 °C under two distinct conditions H_2/air: (1) 50 % RH and 2.5 bar absolute at the anode and 30 % RH and 2.3 bar absolute at the cathode with stoichiometries of 1.4 and 2 respectively, and (2) 80 % RH both sides, 1.5 bar absolute at the anode and 2 bar absolute at the cathode with stoichiometries of 1.5 and 2 respectively. The polarization curves were measured using current steps. The error bars correspond to the voltage variation measured at each step. The results presented in this study should be regarded as preliminary.

3. Ultrasonic decal transfer and welding optimization

Manufacture a MEA using ultrasound process (MEA-US) involves two steps: transferring the electrode onto the membrane to produce the CCM-US, and welding the others components, such as GLDs and subgaskets, to the membrane or the CCM.

Table 1
Parameters (amplitude, energy, stress and trigger force) for transferring electrodes from 250 µm PTFE support to the membrane via ultrasound by sonotrode type using a 35 kHz-1200 W machine from Herrmann.

Sonotrode	Amplitude (µm)	Energy (J/cm^2)	Stress (MPa)	Trigger force (MPa)
4 cm^2	17.9–22.4	35–100	0.125–1.0	0.2
24.6 cm^2	11.7	210–290	0.2	0.04
	12.5	160–200		
	15.6	100–160		
	19.5	60–120		

3.1. Ultrasound-assembled Catalyst Coated Membrane (CCM-US)

During testing transfers, several limitations were identified, particularly concerning the quality of adhesion and the integrity of the components. Criteria were defined to establish the working range limits.

For the lower bound of the range, it was observed that the decal transfer of electrodes from the PTFE support to the membrane was sometimes incomplete. This issue can manifest in two ways: either the entire surface under the sonotrode does not transfer while the center does, or parts of the center do not lift off, leaving missing electrodes on the membrane. Both phenomena reduce the overall quality of the CCM, leading to a reduction in active surface area and a waste of platinum.

For the upper bound of the range, it was observed that the membrane could be degraded during the electrode transfer process. At high energy levels or with inadequate stress parameters, the membrane can flow on the electrodes sides, adhering to the inert PTFE support and causing perforations that render the CCM inoperable.

By optimizing the ultrasonic process parameters, such as ultrasound amplitude, applied stress, and energy supplied, it was possible to transfer electrode surfaces ranging from 4 cm^2 to 24.6 cm^2 (Fig. 2a). The optimized parameter ranges are detailed in Table 1.

The parameters varied depending on the sonotrode used. The amplitudes listed in Table 1 are the only ones explored, and the trigger force, which differs for the two sonotrodes, was not studied.

For the 4 cm^2 sonotrode, electrodes could be transferred to the membrane using the same range of energies and stress levels with an ultrasonic amplitude between 17.9 and 22.4 µm. For the 24.6 cm^2

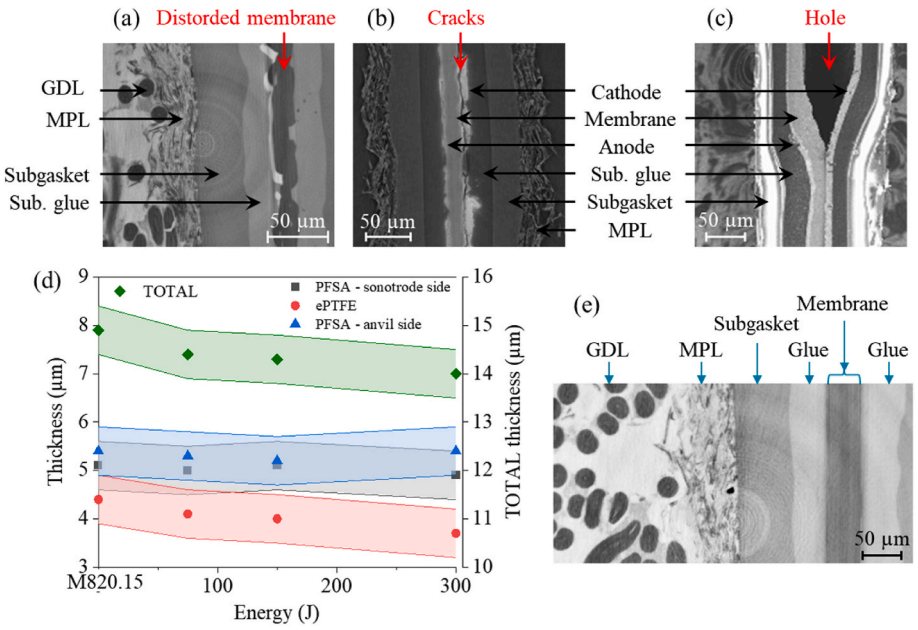

Fig. 3. Key defects in ultrasonic Membrane-Electrode Assembly welding: (a) distorted membrane (1 MPa - 300 J/cm^2) and (b) cracks in the catalyst layers by X-ray tomography (1 MPa - 150 J/cm^2), (c) shrinkage of the sub-gasket adhesive on cooling by SEM (0,5 MPa - 300 J/cm^2), (d) membrane thickness evolution (PFSA-ionomer and ePTFE) as a function of ultrasonic energy up to 300 J at 0.5 MPa. (e) Final MEA components assembly with optimized ultrasound parameters by X-ray tomography (0,5 MPa - 150 J/cm^2).

sonotrode, it is important to note that the ultrasonic amplitude is directly proportional to the energy required for the decal transfers; higher amplitudes require less energy. The stress used with this sonotrode was studied, but successful transfers were only achieved with 0.2 MPa, the maximum stress the ultrasound machine can provide.

To evaluate the quality of the electrode transfer and the integrity of the CCM, the SEM observations were conducted following cross-sectioning via cryo-ultramicrotomy, as illustrated in Fig. 2b. This technique provides a highly uniform surface, essential for accurately measuring changes in the thickness of the CCM.

The SEM observations revealed no significant differences between the CCMs produced by ultrasonic decal transfer and those produced by hot pressing. This suggests that the ultrasonic process is an effective method for producing CCMs of equivalent quality while maintaining the structural integrity of the membrane and the electrodes at this scale. However, a comparison of the membranes before and after decal transfer revealed differences in their thickness.

The thickness of the various layers of the CCM, as depicted in Fig. 2c, was quantified, focusing on the ePTFE reinforcement and the PFSA-ionomer sections on either side of the reinforcement. This analysis was conducted under different mechanical stress conditions and with a fixed ultrasonic energy of 75 J/cm^2. The thickness of the ePTFE, a porous fibrous reinforcement [35,36], was affected by the stress and probably the temperature induced by the ultrasonic process. The ePTFE can deform in thickness due to compaction of its porous structure. In contrast, the PFSA-ionomer sections remained resilient, retaining their original thickness. An illustrative example of a membrane before and after electrode transfer by ultrasound is shown in Supplementary Fig. S2.

It is therefore possible to perform electrode transfers using the two sonotrodes with different surface areas by adjusting the parameters, reducing the time by 94 % compared to the traditional hot-pressing process (2–10 s vs. 180 s).

Scaling up is theoretically possible [23], but it requires optimization of the sonotrode's shape and the surface area exposed to ultrasound, based on the machine specifications and the nature of the components. Initial successful decal transfers (with non-optimized parameters) have also been achieved with a 38 cm^2 sonotrode and one is shown in the supplementary in Fig. S3, demonstrating the capacity to transfer electrodes onto the membrane over several active layer area.

3.2. *Ultrasonic process for Membrane-Electrode Assembly (MEA-US)*

3.2.1. *Optimization of different types of welding*

Manufacture MEA using ultrasound process allows the simultaneous welding of various components including GDLs and subgaskets, to the membrane or CCM, in just a few seconds. This method enables the assembly of up to seven layers (US2, GDL/subgasket/CCM/subgasket/GDL) in a single operation, significantly simplifying the manufacturing process and reducing production time. The application of ultrasonic vibrations facilitates localized fusion at the interface between layers, ensuring a robust and uniform bond without the need for additional binders or elevated temperatures across the entire surface.

However, the ultrasonic process has certain limitations and technical constraints that must be considered to ensure gas-tightness.

Firstly, excessive welding parameters (stress and ultrasonic energy) can cause visible distortion of the membrane and/or cracks in the electrodes, as shown in Fig. 3a and b. This is often due to thermal and mechanical deformation of the components under stress, compromising material integrity and potentially reducing MEA durability.

Secondly, insufficient stress-cooling time after welding can result in partial or total shrinkage of the subgasket adhesive. This phenomenon can cause the membrane electrodes to be pulled out by the adhesive, creating holes at the CCM/adhesive or membrane/adhesive interface, as shown in Fig. 3c. Such holes can compromise the gas-tightness between layers.

Additionally, like in the decal transfer step, increasing the ultrasonic energy during welding can thin the membrane, as shown in Fig. 3d. This thinning is likely due to compression and localized heating caused by ultrasonic vibrations. However, since this thinning occurs outside the active area of the MEA (outside US1), it should not significantly impact the overall performance of the fuel cell.

By optimizing the ultrasonic process parameters, such as ultrasonic energy, applied stress, and cooling time, it is possible to achieve a robust assembly between components without compromising their structural integrity, as shown in Fig. 3e.

It has been demonstrated that a satisfactory assembly can be

Table 2
Parameters (amplitude, energy, stress and trigger force) for welding the different type of components via ultrasound with 4 cm^2 sonotrode using a 35 kHz-1200 W machine from Herrmann.

Welding type	Amplitude (μm)	Energy (J/cm^2)	Stress (MPa)	Trigger force (MPa)
US2 – MEA7	22.4	75–150	0.5	0.2
US3 – MEA5		25–250	0.35–1.25	
US4		12.5–35	0.125–1.25	
US5		12.5–35	0.25–1.25	

achieved between the following components: two GDL and two subgaskets with a membrane in the middle, or two GDL and two subgaskets with a CCM in the center. These assemblies maintain cohesion without significant distortion, preserving the integrity of the membrane, electrode layers, and GDL. Other welds, such as subgasket/membrane/subgasket (US4) and subgasket/subgasket (US5), have also been studied. The optimized parameter ranges depend on the type of the weld, as detailed in Table 2.

Welds were performed using a 4 cm^2 sonotrode with a trigger force of 0.2 MPa and a fixed amplitude of 22.4 μm. The trigger force and amplitude were not studied extensively because ultrasound effectively welds the components over a wide range of energies and stress levels. Below the working ranges, components do not weld together and above these ranges, components exhibit the defects listed previously.

By adjusting the parameters, weld the various components can be performed using the ultrasonic process, reducing processing time by 94 % compared to the traditional hot-pressing method (2–10 s vs. 180 s).

3.2.2. *First MEAs entirely produced by ultrasound*

A fully MEA assembled using ultrasound process was manufactured in a design for a 20 cm^2 cell. A picture is presented in Fig. 4. Areas exposed to ultrasound are hatched. Other folds visible on the MEA were induced by the subgaskets of the technical cell after tests.

The CCM-US used in the center was obtained using the 24.6 cm^2 sonotrode with an amplitude of 15.6 μm and an energy of 100 J/cm^2 with a stress of 0.2 MPa. The decal transfer of the electrodes onto the membrane took 2 s.

The assembly with the others components, a subgasket and a GDL on each side of the CCM-US, was done on the periphery of the GDL. The frame shape of the sonotrode allows avoiding stressing the active area of the assembly. This step took 2.5 s.

In consequence, the whole ultrasound process took around 5 s, which is very fast compared to the 6 min required by hot pressing (CCM manufacturing + GDL and subgasket assembling).

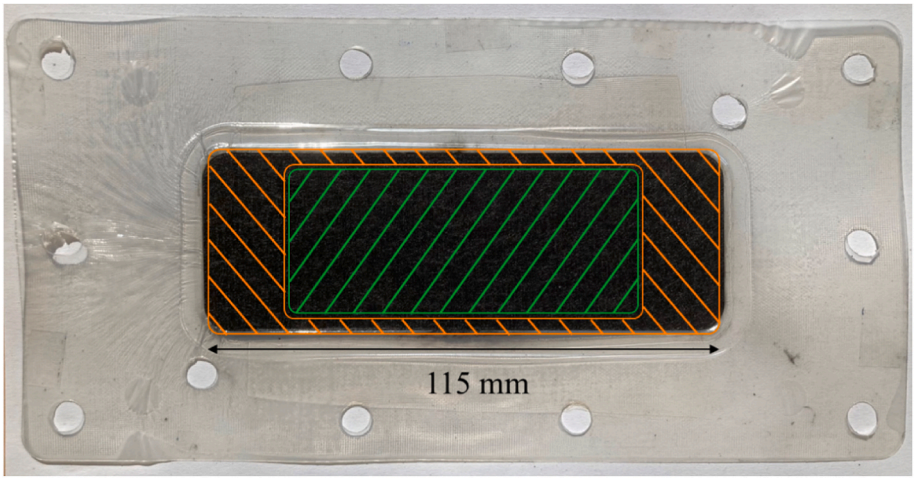

Fig. 4. Picture of an ultrasound-assembled MEA in a 20 cm^2 design after technical mono-cell test, showing the electrode transfer area (green hatching) and the assembly area (orange hatching). (For interpretation of the references to colour in this figure legend, the reader is referred to the Web version of this article.)

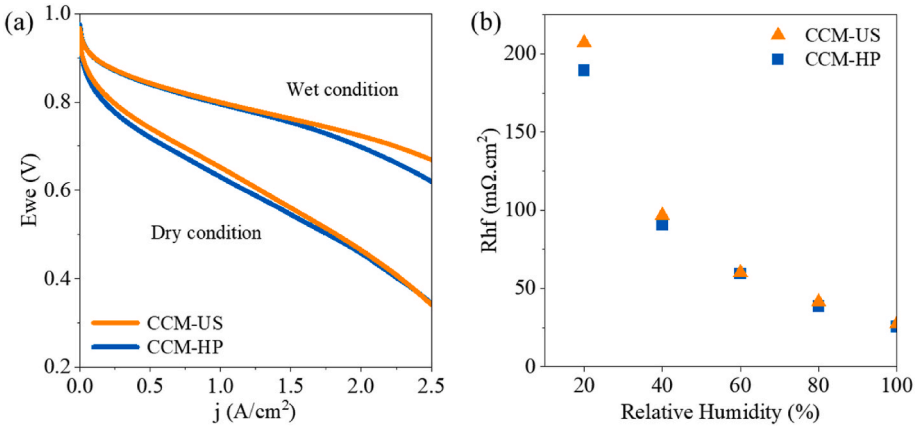

Fig. 5. Comparison of (a) Polarization curve (forward) at 80 °C, H_2/air (38/95 Nl/h) under wet conditions (90 % RH, 2.5 bar absolute) and dry conditions (40 % RH, 1.2 bar absolute) and (b) high-frequency resistance (Rhf) under H_2/N_2 at OCV at different relative humidity (20–100 %) of CCM-US and CCM-HP obtained in 1.8 cm^2 differential cell.

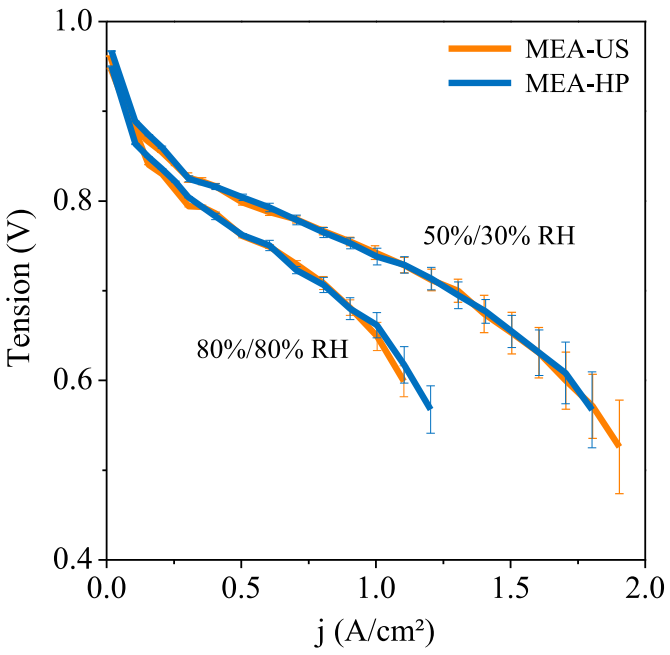

Fig. 6. Comparison of polarization curves (forward) at 80 °C under H_2/air in a 20 cm^2 technical mono-cell. Two distinct conditions are used: (1) 50 % RH and 2.5 bar absolute at the anode and 30 % RH and 2.3 bar absolute at the cathode with stoichiometries of 1.4 and 2 respectively, and (2) 80 % RH both sides, 1.5 bar absolute at the anode and 2 bar absolute at the cathode with stoichiometries of 1.5 and 2 respectively. The error bars correspond to the voltage variation measured at each step during the test.

4. Preliminary performance in 1.8 cm^2 differential cell and in a 20 cm^2 technical mono-cell

4.1. CCM-US vs CCM-HP in 1.8 cm^2 differential cell

The polarization curves of CCM-US and CCM-HP, with 1.8 cm^2 of active surface, shown in Fig. 5a, were measured at 80 °C under two distinct relative humidity (RH) conditions: 90 % RH at 2.5 bar (wet conditions) and 40 % HR at 1.2 bar (dry conditions). The polarization curves shown in the main text correspond to the forward scans, while full forward and reverse polarization curves are provided in the supplementary information as Fig. S4. A more comprehensive study will be proposed in a subsequent paper.

The electrochemical performance of CCM-US and CCM-HP, as shown by polarization curves in Fig. 5a, varies significantly between wet and dry conditions. At 90 % RH, performance improves compared to dry conditions due to enhanced proton conduction in the membrane and in the ionomer of the electrodes, increasing fuel cell efficiency. Preliminary results indicate that the performances of CCM-US and CCM-HP remain similar regardless of humidity levels. Consequently, the thinning of the ePTFE reinforcement at the center of the membrane, caused by the ultrasonic electrode transfer process, does not appear to affect performance.

Fig. 5b presents the high-frequency resistance (Rhf) of these CCMs measured under H_2 at the anode side and N_2 at the cathode side, and at OCV. As humidity increases, Rhf decreases. At low humidity levels, the values for the two CCMs differ, with CCM-US showing the highest resistance (207 mΩ cm^2) at 20 % RH, followed by CCM-HP (190 mΩ cm^2). However, at 40 % RH, the values converge, with CCM-US at 97 mΩ cm^2 and CCM-HP at 91 mΩ cm^2, remaining almost identical at higher humidity levels.

4.2. MEA-US vs MEA-HP in 20 cm^2 technical mono-cell

Polarization curves were also recorded using a 20 cm^2 single-cell setup, as shown in Fig. 6. MEAs prepared via ultrasonic welding and hot pressing were tested at 80 °C under two distinct conditions H_2/air. The results presented in this study should be regarded as preliminary.

The results obtained in the single-cell setup show similar performance between the MEA-US and MEA-HP. These initial findings are consistent with previous results obtained in differential cells under various operable conditions. They are very promising and suggest that the nature of the components has a greater impact than the assembly method used.

The ultrasonic process for manufacturing CCMs appears to be an efficient method of reducing production time by over 94 % compared to hot-pressing process. However, further research is necessary to determine whether the ultrasonic process effects the materials' structure.

5. Conclusions

The ultrasonic process for MEA assembly in PEMFC is a rapid and efficient two-step method, significantly reducing assembly time (94 % in total) and minimizing equipment requirements compared to hot pressing (no additional molds, embossing tools, or positioning templates). The process involves transferring the electrode to the membrane to form the CCM-US, followed by welding additional components, such as GDLs and sub-gaskets, to produce the final MEA-US. The ultrasonic welding of GDLs onto the sub-gaskets in PEMFCs is an innovative step that, to the best of our knowledge, has not yet been implemented in the industry and has been the subject of a patent filed by our team [27].

Successful electrode transfers have been demonstrated using rectangular sonotrodes of various sizes (4 cm^2 and 24.6 cm^2). Scaling up is also possible, as shown by the picture of the 38 cm^2 CCM in the Supplementary Fig. S3. The assembly of multilayer structures (up to seven layers) has been validated with a 4 cm^2 sonotrode. Proof of concept of a MEA-US adapted to a 20 cm^2 technical cell has been demonstrated. The MEA-US assembly took only 5 s.

Preliminary electrochemical performance data indicate that CCMs manufactured by the ultrasonic process match conventionally assembled CCMs, even under varying humidity conditions, underscoring the potential of this technique for PEMFC manufacturing. Polarization curves measured in a 20 cm^2 technical single cell showed similar performance for the MEA-US and MEA-HP.

However, several limitations must be addressed before considering broader implementation. While the feasibility of scaling to 38 cm^2 has been demonstrated visually, electrochemical performance at this size remains untested. In the context of large active areas (≥1000 cm^2) required for automotive MEAs, such scaling could be achievable by adapting the anvil design, sonotrode characteristics and process parameters. Moreover, the process also depends on manual alignment, which could affect reproducibility in automated manufacturing environments. Finally, long-term durability and mechanical integrity under fuel cell cycling conditions have yet to be evaluated.

Further research is needed to explore the effects of ultrasonic processing on ionomer structure, particularly its impact on proton conduction and material durability, which are critical parameters for ensuring long-term performance. While the ultrasonic approach was demonstrated in this study for a specific set of components, additional tests using alternative materials (such as different membranes, GDLs, subgaskets, and ink compositions) have further highlighted the versatility of this technology.

CRediT authorship contribution statement

Claire Tougne: Writing – review & editing, Writing – original draft, Visualization, Methodology, Investigation, Formal analysis, Data curation, Conceptualization. **Thomas Cavoué:** Writing – review & editing,

Formal analysis, Data curation. **Arnaud Morin:** Writing – review & editing, Validation, Supervision, Project administration, Methodology, Formal analysis, Conceptualization. **Christine Nayoze-Coynel:** Writing – review & editing, Validation, Supervision, Resources, Project administration, Methodology, Investigation, Funding acquisition, Formal analysis, Conceptualization.

Declaration of competing interest

The authors declare the following financial interests/personal relationships which may be considered as potential competing interests: Christine Nayoze-Coynel reports financial support was provided by ANR Carnot Energies du futur. Christine Nayoze-Coynel and Claire Tougne have patent #FR2403696 issued to CEA. If there are other authors, they declare that they have no known competing financial interests or personal relationships that could have appeared to influence the work reported in this paper.

Acknowledgments

The authors acknowledge SOLEIL for provision of synchrotron radiation facilities and we would like to thank Dr. Mario Scheel and Dr. Timm Weitkamp for assistance in using beamline ANATOMIX (proposal No. 20230003). ANATOMIX is an Equipment of Excellence (EQUIPEX) funded by the Investments for the Future program of the French National Research Agency (ANR), project NanoimagesX, grant no. ANR-11-EQPX-0031. We thank the European Synchrotron Radiation Facility (ESRF) for access to its facilities (proposal No. MA5952), as well as the technical team for their support on beamline ID16B. Finally, we also thank the ANR Carnot "Energies du futur" for having funded this work under the project FAMEOUS.

Appendix A. Supplementary data

Supplementary data to this article can be found online at https://doi.org/10.1016/j.jpowsour.2025.238061.

Data availability

Data will be made available on request.

References

[1] H. Lee, J. Romero, Climate Change 2023 Synthesis Report IPCC, 2023: Sections. In: Climate Change 2023: Synthesis Report. Contribution of Working Groups I, II and III to the Sixth Assessment Report of the Intergovernmental Panel on Climate Change [Core Writing Team, (n.d.) 35–115. https://doi.org/10.59327/IPCC/AR6-9789291691647..

[2] M.K. Singla, P. Nijhawan, A.S. Oberoi, Hydrogen fuel and fuel cell technology for cleaner future: a review, Environ. Sci. Pollut. Control Ser. 28 (13) (2021) 15607–15626, https://doi.org/10.1007/S11356-020-12231-8, 28 (2021.

[3] A. Soleimani, S.H. Hosseini Dolatabadi, M. Heidari, A. Pinnarelli, B. Mehdizadeh Khorrami, Y. Luo, P. Vizza, G. Brusco, Progress in hydrogen fuel cell vehicles and up-and-coming technologies for eco-friendly transportation: an international assessment, Multiscale and Multidisciplinary Modeling, Experiments Design 7 (2024) 3153–3172, https://doi.org/10.1007/S41939-024-00482-8/TABLES/1.

[4] F. van der Linden, E. Pahon, S. Morando, D. Bouquain, F. Van Der Linden, E. Pahon, S. Morando, D. Bouquain, A review on the Proton-Exchange Membrane Fuel Cell break-in physical principles, activation procedures, and characterization methods, J. Power Sources 575 (2023) 233168, https://doi.org/10.1016/j.jpowsour.2023.233168i.

[5] D.K. Madheswaran, M. Thangamuthu, S. Gnanasekaran, S. Gopi, T. Ayyasamy, S. S. Pardeshi, Powering the future: progress and hurdles in developing proton exchange membrane fuel cell components to achieve department of energy goals—a systematic review, Sustainability 15 (2023) 15923, https://doi.org/10.3390/SU152215923, 15923 15 (2023).

[6] A.G. Abokhalil, M. Alobaid, A. Al Makky, Innovative approaches to enhance the performance and durability of proton exchange membrane fuel cells, Energies 16 (2023) 5572, https://doi.org/10.3390/EN16145572, 5572 16 (2023).

[7] S. Mo, L. Du, Z. Huang, J. Chen, Y. Zhou, P. Wu, L. Meng, N. Wang, L. Xing, M. Zhao, Y. Yang, J. Tang, Y. Zou, S. Ye, Recent advances on PEM fuel cells: from key materials to membrane electrode assembly, Electrochem. Energy Rev. 6 (1) (2023) 1–37, https://doi.org/10.1007/S41918-023-00190-W, 6 (2023).

[8] M. Grandi, S. Rohde, D.J. Liu, B. Gollas, V. Hacker, Recent advancements in high performance polymer electrolyte fuel cell electrode fabrication – novel materials and manufacturing processes, J. Power Sources 562 (2023) 232734, https://doi.org/10.1016/J.JPOWSOUR.2023.232734.

[9] Q. Meyer, N. Mansor, F. Iacoviello, P.L. Cullen, R. Jervis, D. Finegan, C. Tan, J. Bailey, P.R. Shearing, D.J.L. Brett, Investigation of hot pressed polymer electrolyte fuel cell assemblies via X-ray computed tomography, Electrochim. Acta 242 (2017) 125–136, https://doi.org/10.1016/J.ELECTACTA.2017.05.028.

[10] U.A. Hasran, S.K. Kamarudin, W.R.W. Daud, B.Y. Majlis, A.B. Mohamad, A.A. H. Kadhum, M.M. Ahmad, Optimization of hot pressing parameters in membrane electrode assembly fabrication by response surface method, Int. J. Hydrogen Energy 38 (2013) 9484–9493, https://doi.org/10.1016/J.IJHYDENE.2012.12.054.

[11] D. Ramani, N.S. Khattra, Y. Singh, F.P. Orfino, M. Dutta, E. Kjeang, Mitigation of mechanical membrane degradation in fuel cells – Part 2: bonded membrane electrode assembly, J. Power Sources 512 (2021) 230431, https://doi.org/10.1016/J.JPOWSOUR.2021.230431.

[12] Z.X. Liang, T.S. Zhao, C. Xu, J.B. Xu, Microscopic characterizations of membrane electrode assemblies prepared under different hot-pressing conditions, Electrochim. Acta 53 (2007) 894–902, https://doi.org/10.1016/J.ELECTACTA.2007.07.071.

[13] J. Beck, Ultrasonic Bonding of Membrane Electrode Assemblies for Low Temperature Proton Exchange Membrane Fuel Cells, 2012.

[14] J. Beck, D. Walczyk, C. Hoffman, S. Buelte, Ultrasonic bonding of membrane electrode assemblies for low temperature proton exchange membrane fuel cells, J. Fuel Cell Sci. Technol. 9 (2012), https://doi.org/10.1115/1.4007136/372064.

[15] D. Walczyk, R. Puffer, Adaptive Process Controls and Ultrasonics for High Temperature PEM MEA Manufacture,, 2015.

[16] H. Dohle, V. Peincke, I. Busenbender, T. Kels, Method for Producing a Membrane with an Electrode Applied Ultrasonically, 1998.

[17] T. Snelson, R. Puffer, D. Walczyk, J. Pyzza, L. Krishnan, Method for the Production of an Electrochemical Cell, 2011.

[18] L. Hoon Hui, Method for Manufacturing Fuel Cell Membrane-Electrode Assembly Ultrasonic Vibration Bonding, 2011.

[19] L. Whonhee, The Sub-gasket Adhesion Method for Fuel Cell Membrane Electrode Assembly Production Using Ultrasonic Vibration, 2013. KR10-2013-0033581 A.

[20] M. Fritz, P. Clausnitzer, J. Roser, Fuel Cell and Roll-To-Roll Process to Manufacture Fuel Cell Assembly with Electrical Membrane Units Ultrasonically Welded to Surrounding Frame, 2007. DE102005058370 A1.

[21] R. Fukui, Method for Manufacturing Membrane Electrode Assemblies and Membrane Electrode Assemblies and Polymer Electrolyte Fuel Cells, 2008.

[22] K. Katsuhiko, Manufacturing Apparatus for Fuel Battery Cell, 2018.

[23] D.A. Wang, Ultrasonic bonding of membrane-electrode-assemblies of fuel cells, Int. J. Adv. Sci. Eng. Inf. Technol. 6 (2016) 281–284, https://doi.org/10.18517/IJASEIT.6.3.804.

[24] T.G. Unnikrishnan, P. Kavan, A review study in ultrasonic-welding of similar and dissimilar thermoplastic polymers and its composites, Mater. Today Proc. 56 (2022) 3294–3300, https://doi.org/10.1016/J.MATPR.2021.09.540.

[25] S.K. Bhudolia, G. Gohel, K.F. Leong, A. Islam, Advances in ultrasonic welding of thermoplastic composites: a review, Materials 13 (2020) 1284, https://doi.org/10.3390/ma13061284.

[26] X. Fu, X. Yuan, G. Li, Y. Wu, H. Tong, S. Kang, J. Luo, Z. Pan, W. Lu, A study on ultrasonic welding of thermoplastics with significant differences in physical properties under different process parameters, Mater. Today Commun. 33 (2022) 105009, https://doi.org/10.1016/J.MTCOMM.2022.105009.

[27] C. Tougne, C. Siguenza, C. Nayoze-Coynel, Assemblage pour pile à combustible et procédé de fabrication d'un tel assemblage, 2025. FR2403696.

[28] T. Weitkamp, M. Scheel, J. Perrin, G. Daniel, A. King, V. Le Roux, J.L. Giorgetta, A. Carcy, F. Langlois, K. Desjardins, C. Menneglier, M. Cerato, C. Engblom, G. Cauchon, T. Moreno, C. Rivard, Y. Gohon, F. Polack, Microtomography on the ANATOMIX beamline at synchrotron SOLEIL, J. Phys Conf. Ser. 2380 (2022) 012122, https://doi.org/10.1088/1742-6596/2380/1/012122.

[29] T. Weitkamp, M. Scheel, J.L. Giorgetta, V. Joyet, V. Le Roux, G. Cauchon, T. Moreno, F. Polack, A. Thompson, J.P. Samama, The tomography beamline ANATOMIX at Synchrotron SOLEIL, J. Phys Conf. Ser. 849 (2017) 012037, https://doi.org/10.1088/1742-6596/849/1/012037.

[30] A. Mirone, E. Brun, E. Gouillart, P. Tafforeau, J. Kieffer, The PyHST2 hybrid distributed code for high speed tomographic reconstruction with iterative reconstruction and a priori knowledge capabilities, Nucl. Instrum. Methods Phys. Res. B 324 (2014) 41–48, https://doi.org/10.1016/J.NIMB.2013.09.030.

[31] G. Martinez-Criado, J. Villanova, R. Tucoulou, D. Salomon, J.P. Suuronen, S. Laboure, C. Guilloud, V. Valls, R. Barrett, E. Gagliardini, Y. Dabin, R. Baker, S. Bohic, C. Cohen, J. Morse, ID16B: a hard X-ray nanoprobe beamline at the ESRF

for nano-analysis, J. Synchrotron Radiat. 23 (2016) 344–352, https://doi.org/10.1107/S1600577515019839.
[32] P. Cloetens, W. Ludwig, J. Baruchel, D. Van Dyck, J. Van Landuyt, J.P. Guigay, M. Schlenker, Holotomography: quantitative phase tomography with micrometer resolution using hard synchrotron radiation x rays, Appl. Phys. Lett. 75 (1999) 2912–2914, https://doi.org/10.1063/1.125225.
[33] V. Favre-Nicolin, G. Girard, S. Leake, J. Carnis, Y. Chushkin, J. Kieffer, P. Paléo, M.-I. Richard, PyNX: high performance computing toolkit for coherent X-ray imaging based on operators, J. Appl. Crystallogr. 53 (2020) 1404–1413, https://doi.org/10.1107/S1600576720010985.
[34] P. Paleo, J. Lesaint, H. Payno, A. Mirone, N. Vigano, C. Nemoz, Nabu 2024.1. https://doi.org/10.5281/ZENODO.11104029, 2024.
[35] G. ePTFE P.A. Industry, The Role of an ePTFE-Reinforced Polymer Electrolyte Membrane (PEM) in the Automotive Fuel Cell Market, (n.d.). .
[36] HP15 ePTFE Reinforced PFSA Membrane, (n.d.). https://www.fuelcellstore.com/eptfe-reinforced-pfsa-membrane-15-microns (accessed October 9, 2024) .